JOURNAL OF APPLIED ELECTROCHEMISTRY 18 (1988) 384–393

Electrochemical behaviour of copper in neutral aerated chloride solution. II. Impedance investigation

CLAUDE DESLOUIS, BERNARD TRIBOLLET

LP 15 du CNRS 'Physique des Liquides et Electrochimie' associé à l'Université Pierre et Marie Curie, 4 place Jussieu, 75252 Paris Cedex 05, France

GUILIANO MENGOLI, MARCO M. MUSIANI

Istituto di Polarografia ed Elettrochimica Preparativa del CNR, Corso Stati Uniti, 4. 35100 Padova, Italy

Received 10 July 1987; revised 2 October 1987

A.c. and EHD impedance measurements were performed on a Cu rotating disc electrode immersed in neutral aerated NaCl and the results were compared with simulated curves according to the kinetic model developed in Part I. The agreement is good over the whole anodic range and at the corrosion potential. A slowing down of the mass transport rate is explained by diffusion through a surface layer (Cu_2O) at the corrosion potential and for the close anodic range. It is confirmed that, on the cathodic plateau, the interface may be considered as uniformly accessible for the cathodic partial reaction of oxygen reduction. However, at less cathodic potential a surface layer effect due to CuCl must also be taken into account. Diffusion coefficients for both O_2 and $CuCl_2^-$ were determined by EHD impedance.

1. Introduction

Corrosion and electrodissolution of Cu in neutral aerated NaCl were investigated in Part I of this work by using steady-state techniques [1]. An analysis of the results obtained led us to propose a mechanism for the electrodissolution of Cu which appears better than previous ones [2–6] in its ability to explain the dependence of anodic current on $[Cl^-]$.

By investigating the corrosion process, it was established that at least two different insoluble corrosion products are formed at E_{corr}, i.e. CuCl and Cu_2O, the former being produced rapidly and the latter being the main component of surface layers after a long time of immersion in the NaCl solutions. The hypothesis was put forward that the growth of such a layer hinders mass transfer and, in turn, lowers the corrosion current (which was found to depend on the rotation rate of the electrode). However, an effect of a porous layer on the rate of mass transfer is not the only possible explanation for the results close to the corrosion potential described in Part I. The calculation of I_{corr} was done in Part I by assuming that only the anodic partial reaction is mass transfer-limited at E_{corr}. If this is true, the surface layer will only influence anodic mass transfer at the corrosion potential.

In order to clarify these points and to further check the proposed mechanism, the corrosion and electrodissolution of Cu in neutral aerated 0.5 M NaCl were studied by impedance techniques, both electrochemical (a.c.) and electrohydrodynamical (EHD).

Impedance plots for Cu in neutral NaCl were published by Heakal and Haruyama [7] and by Mansfield *et al.* [8] with only very little comment since, in both instances, they were used as a reference for benzotriazole-inhibited Cu. More recently Smyrl [5] has investigated the a.c. impedance response of Cu in acidic chloride media.

EHD impedance, i.e. the frequency response of the system to a perturbation of the angular speed of the electrode [9–13], was applied here to Cu for the first time. Two EHD impedances can be defined: one in potentiostatic regulation $(dI/d\Omega)_E$ and one in galvanostatic regulation $(dE/d\Omega)_I$. These two impedances are linked to the usual a.c. impedance $(dE/dI)_\Omega$ by the relationship [14]:

$$(dE/d\Omega)_I = -(dE/dI)_\Omega (dI/d\Omega)_E \quad (1)$$

or by using another notation:

$$\tilde{E} = Z\tilde{I} + Z_{EHD}\tilde{\Omega} \quad (2)$$

where $Z = (dE/dI)_\Omega$ and $Z_{EHD} = (dE/d\Omega)_I$. Following the local slope of the current–potential curve, the EHD impedance in potentiostatic or galvanostatic regulation will be measured. For example, on the diffusion plateau a potentiostatic regulation will be chosen and a galvanostatic regulation at E_{corr}.

For a fast redox reaction on a uniformly accessible electrode, the EHD impedance diagrams obtained at different rotation rates can be reduced using the dimensionless frequency $p = \omega/\bar{\Omega}$ (where ω is the modulation frequency and $\bar{\Omega}$ the mean rotation frequency); when the frequency tends towards infinity the phase shift tends towards 180° in potentiostatic regulation or 225° in galvanostatic regulation. For a fast redox reaction occurring at an interface covered by a porous nonreactive layer the concentration gradient is distributed between the fluid and the porous layer. Then, the EHD impedance is not reduced by the dimensionless frequency as shown in Fig. 1 [15]. The lower the mean rotation rate $\bar{\Omega}$, the closer to the EHD impedance diagram on a bare

0021-891X/88 $03.00 + .12 © 1988 Chapman and Hall Ltd.

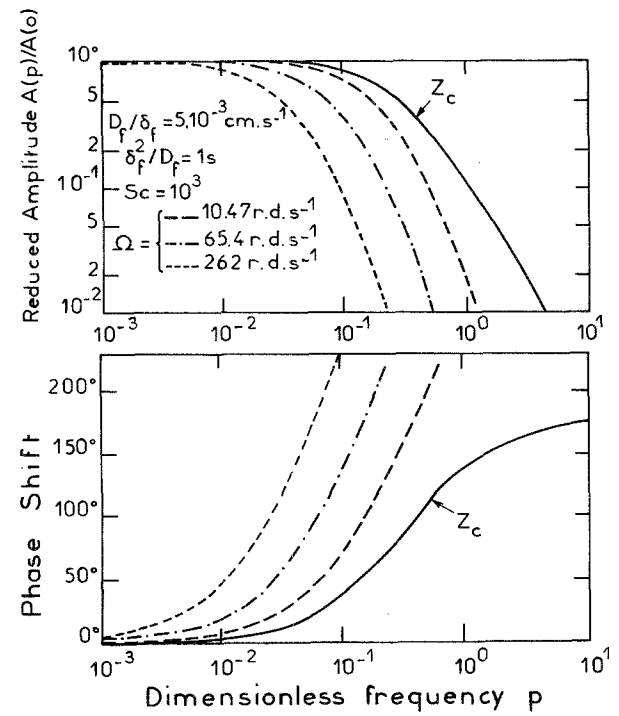

Fig. 1. Variation of the theoretical impedance vs the dimensionless frequency p in Bode coordinates, for an interface covered with a porous layer of thickness δ_f. The diffusion coefficient in the layer is D_f.

electrode is the corresponding diagram. The phase shift increases infinitely with p and no asymptotic value is reached.

For a fast redox reaction occurring on a partially blocked electrode characterized by alternating active and passive sites, the EHD impedance diagram is reported in Fig. 2 [16]. In the low frequency range, the frequency response corresponds to that of the rotating disc electrode with a uniform active surface (diagram reduced by p); in the high frequency range, the frequency response corresponds to that of an isolated active site (diagram reduced by p). The translation

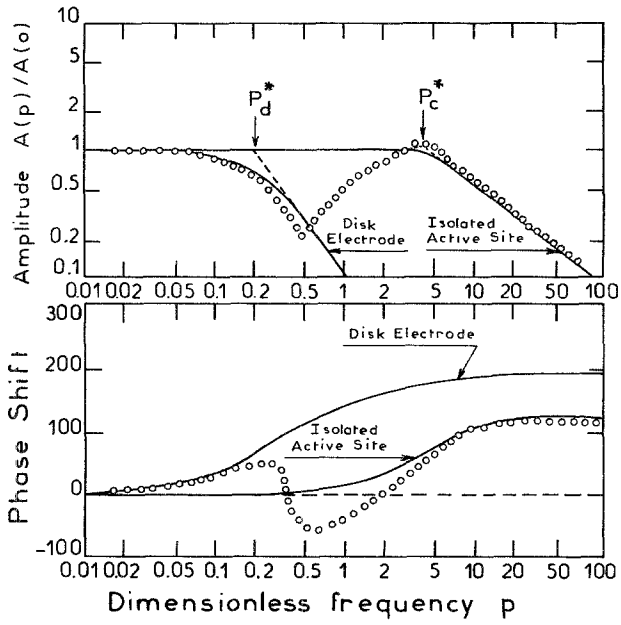

Fig. 2. Variation of the theoretical EHD impedance vs the dimensionless frequency, in Bode coordinates, for a partially active surface.

between the two asymptotes (disc and isolated active site) is a function of the active site geometry and independent of the gap value between two active sites. The gap value affects only the transition between the two limiting curves; for this transition, in the middle frequency range, all curves are not reduced by p.

2. Experimental details

The chemicals and materials used have been described in Part I of this work [1].

Alternating current (a.c.) impedance measurements were made using a Solartron 1250 frequency response analyser and a Solartron 1186 electrochemical interface, covering a wide frequency range (10 mHz–63 kHz). Five to 10 mV (rms) a.c. potential perturbations were used in potentiostatic experiments in order to ensure linearity. Data were acquired and processed by an Olivetti M24 computer.

The equipment used for EHD impedance experiments has been described in detail elsewhere [10, 13].

3. Impedance calculation

The following calculation is obtained from the steady-state model described in Part I (Equations 2, 14 and 15). Now we assume that the state of the electrochemical system is sinusoidally modulated around a mean value in a linear way such that any time-dependent variable of the system (i, E, [CuCl], $[CuCl_2^-]$, Ω) performs harmonic variations and so may be written in the following form:

$$X = \bar{X} + \tilde{X} \exp(j\omega t) \tag{3}$$

where $\tilde{X}$ is a complex quantity and $\omega/2\pi$ is the modulation frequency.

The set of Equations 2, 14 and 15 given in Part I becomes:

$$\tilde{i}/F = R_t^{-1}\tilde{E} - k_{-1} \times \exp(-(1-\alpha)F\bar{E}/RT)[\widetilde{CuCl}] \tag{4}$$

$$j\omega[\widetilde{CuCl}] = R_t^{-1}\tilde{E} - k_{-1} \times \exp(-(1-\alpha)F\bar{E}/RT)[\widetilde{CuCl}] - k_2[\overline{Cl^-}][\widetilde{CuCl}] + k_{-2}[\widetilde{CuCl_2^-}] \tag{5}$$

$$\tilde{i}/F = D(\mathrm{d}[\widetilde{CuCl_2^-}]/\mathrm{d}y)_0 \tag{6}$$

where R_t, the charge transfer resistance, is:

$$R_t^{-1} = (\alpha F/RT)k_1[\overline{Cl^-}] \exp(\alpha F\bar{E}/RT) + ((1-\alpha)F/RT)k_{-1}[\widetilde{CuCl}] \times \exp((1-\alpha)F\bar{E}/RT) \tag{7}$$

$[\widetilde{CuCl_2^-}]$ and $(\mathrm{d}[\widetilde{CuCl_2^-}]/\mathrm{d}y)_0$ are linked by the relation-

ship given in a similar form in [11]:

$$[\widetilde{CuCl_2^-}] = \delta(-1/\theta'(o))(d[\widetilde{CuCl_2^-}]/dy)_0 - \delta(-1/\theta'(o))Z_c\tilde{\Omega} \quad (8)$$

where $(-1/\theta'(o))$ is the usual dimensionless convective Warburg impedance (also called diffusion impedance) [17, 18] and Z_c is proportional to the EHD impedance in 'concentrostatic' regulation and is studied in detail in Ref. [11].

By eliminating $[\widetilde{CuCl}]$, $[\widetilde{CuCl_2^-}]$ and $(d[\widetilde{CuCl_2^-}]/dy)_0$, the general expression between the observable quantities is written in the form of Equation 2:

$$R_t^{-1}\tilde{E} = \{1 + [k_{-1}\exp(-(1-\alpha)F\bar{E}/RT)]/(j\omega + k_2[\overline{Cl^-}]) + [k_{-1}\exp(-(1-\alpha)F\bar{E}/RT) \times k_{-2}\delta(-1/\theta'(o))/D(j\omega + k_2[\overline{Cl^-}])\}\tilde{i}/F - [k_{-1}\exp(-(1-\alpha)F\bar{E}/RT) \times k_{-2}\delta(-1/\theta'(o))Z_c/(j\omega + k_2[\overline{Cl^-}])\tilde{\Omega} \quad (9)$$

With $\tilde{\Omega} = 0$ we obtain the a.c. electrochemical impedance which appears as clearly described by three loops more or less decoupled.

With $\tilde{i} = 0$ we obtain directly the expression of the EHD impedance in galvanostatic regulation.

4. Results and discussion

4.1. *Cathodic range*

4.1.1. A.c. impedance. A.c. impedance diagrams obtained at −500 mV (SCE), i.e. at a potential between the cathodic plateau and the reduction peak of CuCl, are shown in Fig. 3. At each rotation rate they may be described by two loops poorly resolved. The one corresponding to the low frequency range, is due to mass transfer since its characteristic frequency depends linearly on Ω. A plot of the imaginary part vs the dimensionless frequency $p = \omega/\bar{\Omega}$ on a bilogarithmic scale indicates no shift of the curves obtained at different rotation rates, i.e. the mass transfer entirely occurs in the fluid [15]. The loop corresponding to the high frequency range is ascribed to the combination of charge transfer resistance and the double layer capacitance. From the impedance measurement in the higher frequency range the double layer capacitance value has been determined ($C_d = 35\,\mu F\,cm^{-2}$).

We notice that the R_p values, i.e. the limit of Z when ω tends towards zero, are in agreement with the slopes of the current potential curves (Fig. 1, Part I).

4.1.2. EHD impedance. EHD impedances in potentiostatic regulation have been performed at the diffusion cathodic plateau for two different potentials, −900 and −750 mV (SCE), the latter potential being clearly less cathodic than the reduction peak of Cu_2O (Fig. 1, Part I). Experimental data are reported in Fig. 4 in Bode coordinates, i.e. the amplitude and phase shifts of the quantity $\tilde{I}/\tilde{\Omega}$ vs the dimensionless frequency $p = \omega/\bar{\Omega}$. The points fall on a single curve for $p \leqslant 2$ whatever the potential, a fact which is consistent with a reduction in conditions of uniform accessibility, the reduced species here being oxygen.

A quantitative comparison with the theory [11] was done by performing a non-linear fitting procedure with only one adjustable parameter: the Schmidt number of the electroactive species $Sc = \nu/D$. The agreement between the theoretical expression and experimental data was consistent with a relative experimental error around 3%. The results of the fitted values are reported in Table 1. From the Sc values we deduced a mean D value of $1.4 \times 10^{-5}\,cm^2\,s^{-1}$ which is smaller than that provided by the steady state measurements ($2 \times 10^{-5}\,cm^2\,s^{-1}$) but of the same order of magnitude and corresponding to a number of 4 electrons transferred in the cathodic reduction of oxygen. One source of discrepancy may arise from the fact that no assumption is necessary here about the solubility of oxygen which was used for the steady state measurements. However both values are in agreement with existing data [19].

For $p > 2$ a decrease of the phase shift and a small increase of the amplitude are at variance with the situation of uniform accessibility for which a limiting phase of 180° and $A(p) \propto p^{-2}$ when $p \to \infty$ must be observed. Such a behaviour was predicted for partially

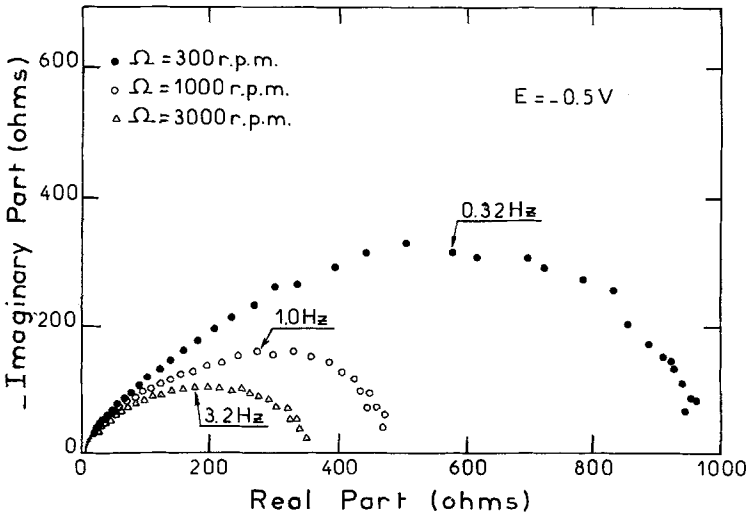

Fig. 3. A.c. impedance in the cathodic range ($E = -500$ mV) obtained for three different rotation rates.

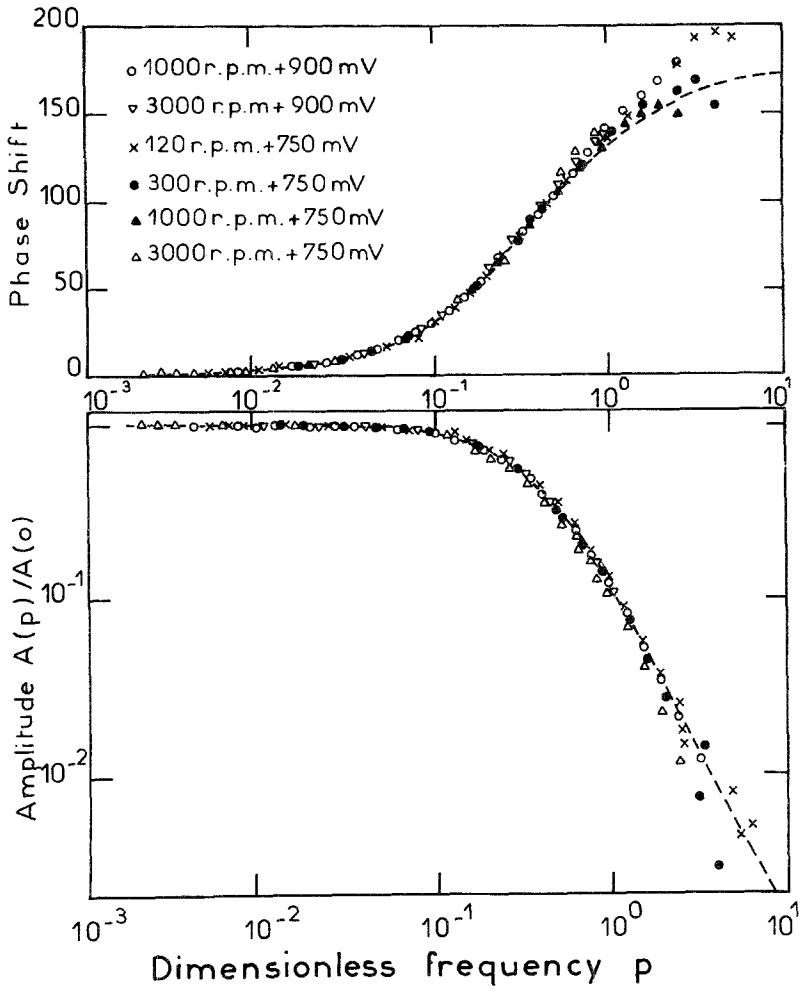

Fig. 4. EHD impedance in potentiostatic regulation at the diffusion plateau obtained for different rotation rates. The theoretical curve corresponding to $Sc = 700$ is reported as a dashed line.

blocked surfaces [16]. However it must be assumed in the present case that the blocked ratio of the surface remains small with respect to the overall area since high frequency modulations are needed to see this effect. These data are in agreement with the steady-state measurement because if the blocked ratio were not negligible I vs $\Omega^{1/2}$ plots (Fig. 3, Part I) would not be straight lines.

When a layer of Cu_2O exists at the copper interface (-750 mV), the behaviour of the interface is still that of a uniformly accessible interface. Then, the oxygen reduction occurs at the Cu_2O–electrolyte interface which means that the layer has no significant barrier effect in this potential range.

Below the limiting current, galvanostatic regulation

Table 1. Best-fit values for the Schmidt number of O_2 from EHD experiments on the cathodic plateau

Potential (mV(SCE))	*Ω (rpm)*	Sc
−900	120	620
−900	300	590
−900	1200	660
−900	3000	690
−750	120	620
−750	300	690

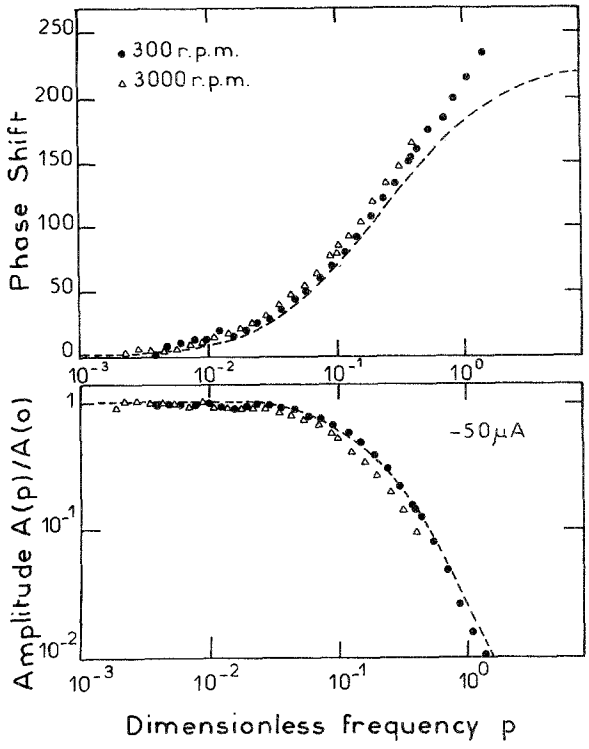

Fig. 5. EDH impedance in galvanostatic regulation below the diffusion plateau ($I = -50\,\mu$A) for two different rotation rates. The theoretical curve corresponding to $Sc = 700$ is reported as a dashed line.

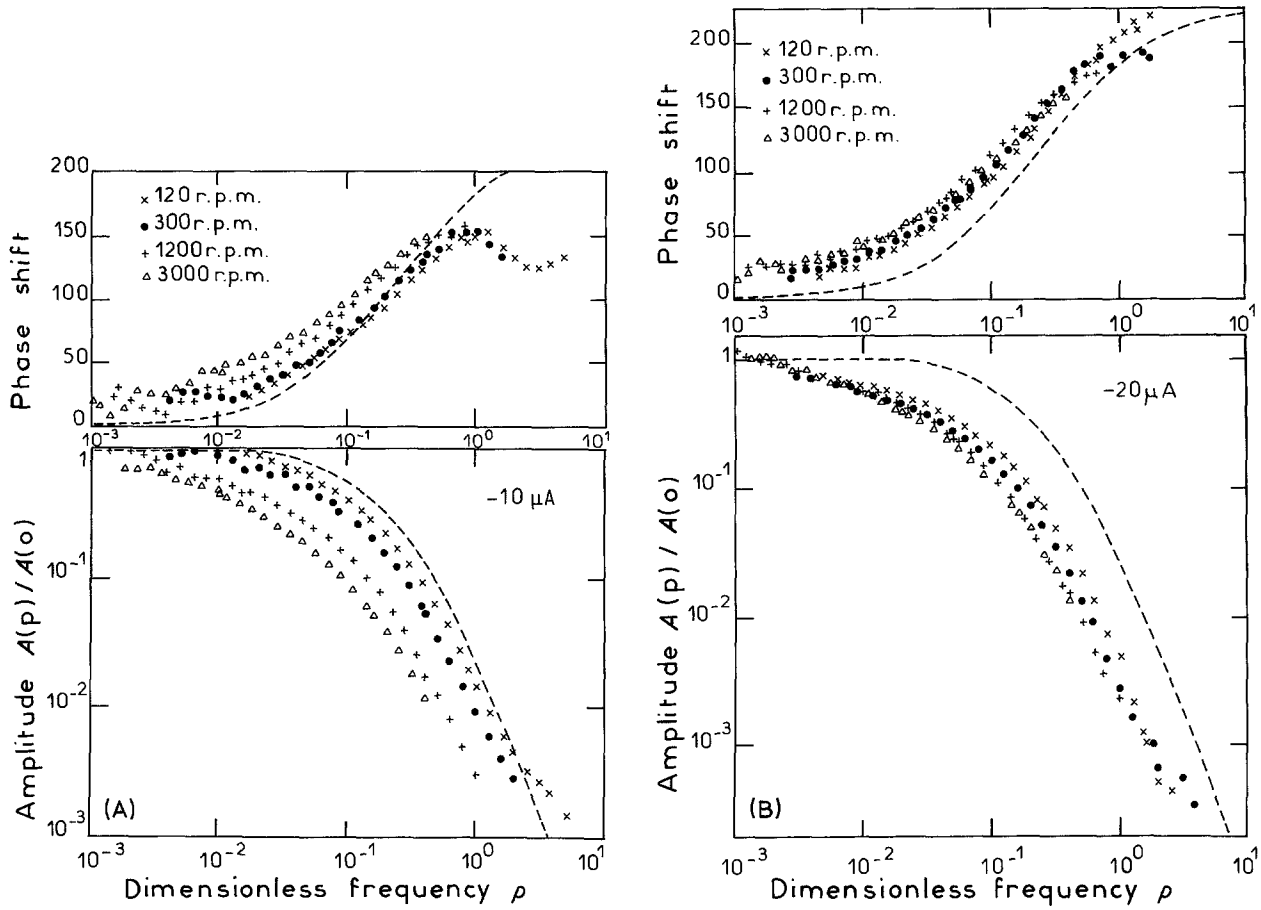

Fig. 6. EDH impedance in galvanostatic regulation below the diffusion plateau ((A) $I = -10\,\mu A$; (B) $I = -20\,\mu A$) for different rotation rates. The theoretical curve corresponding to $Sc = 700$ is reported as a dashed line.

was preferred to the potentiostatic one. For a potential range between -400 and -500 mV (SCE), i.e. at a potential more cathodic than that of a presumed complete reduction of CuCl, the results provide evidence that the conditions for oxygen reduction remain basically the same as those of the plateau. The two curves plotted in Fig. 5 for $I = -50\,\mu A$ at $\bar{\Omega} = 300$ rpm and 3000 rpm are well superimposed at low p and then their separation increases at higher p. This behaviour may be explained by a blocking effect with a small blocking ratio.

On the contrary, measurements performed at lower current, i.e. below the reduction peak of CuCl, present distinct diagrams which are no longer reducible vs p when $\bar{\Omega}$ is varied (Fig. 6A and 6B). The phase shift at very low frequency shows a residual value around 20° which may be due to a slow potential evolution with time (see Fig. 2, Part I). The lack of reducibility with p for different rotation rates may be explained by a layer effect and in this case the layer may only be CuCl. The high frequency behaviour is characteristic of a partially blocked electrode, but such an effect cannot occur with a layer. One possible explanation is to assume that the major part of the interface is covered by CuCl (layer effect) and the smaller part is directly accessible as active site for the oxygen reduction, this smaller part being sensible only in the high frequency range.

4.2. *Anodic range*

4.2.1. A.c. impedance. A.c. impedance diagrams were recorded at -200 and -150 mV (SCE). Those obtained at the latter potential for three values of $\bar{\Omega}$ are shown in Fig. 7 and may be described by three loops relatively well decoupled. Equation 9 derived in the previous section also leads to an a.c. impedance plot consisting of three loops. Simulated curves obtained for the same $\bar{\Omega}$ values, a diffusion coefficient $D = 4.5 \times 10^{-6}$ cm^2 s^{-1} (see below) and appropriate parameters are shown in Fig. 8. The similarity between the simulated and experimental curves is sufficiently good for both the general shape and characteristic frequencies. The main discrepancy is observed at high frequency where the experimental diagrams are more poorly resolved than the simulated ones and the angle formed between the real axis and the curve is less than 90°. Both these facts are possibly explained with dispersion phenomena due to electrode roughness.

Of the three loops, the one at high frequency is due to R_t and double layer capacitance, that at low frequency corresponds to mass transfer, while that at intermediate frequency is due to the modulation of [CuCl].

In the low frequency range, the imaginary part of the impedance is fully reducible vs p confirming a

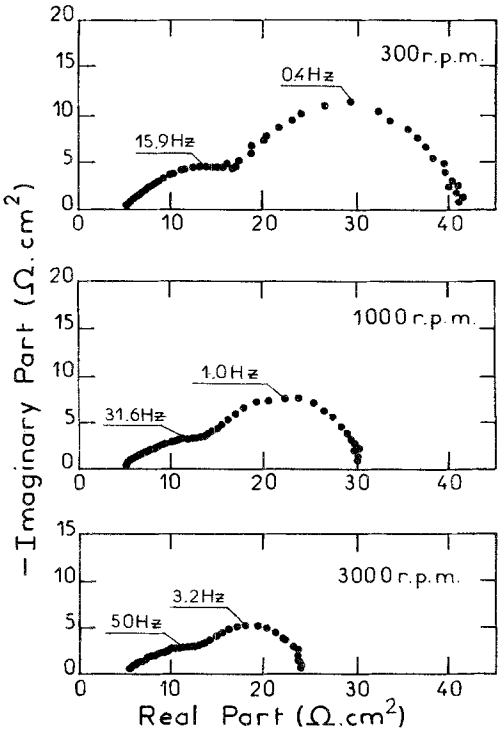

Fig. 7. A.c. impedance diagrams for $E = -150$ mV (SCE) and three different rotation rates. The characteristic frequencies of the first two loops are indicated.

purely mass transport control and giving no indication of mass transfer through a porous layer.

In the mid frequency range, the intermediate loop is independent of $\bar{\Omega}$ from the model while some shift is experimentally found (the characteristic frequency of this loop increases by a factor around 3 when $\bar{\Omega}$ is varied from 300 to 3000 rpm).

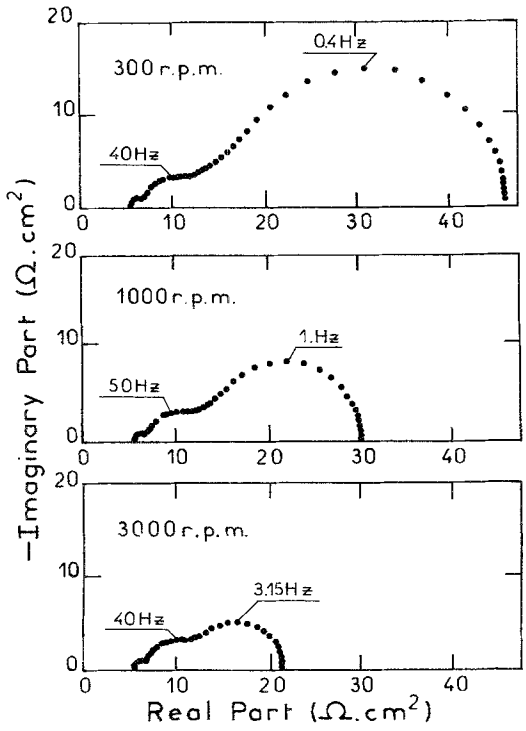

Fig. 8. Simulated a.c. impedance diagrams from Equation 9 with $R_t = 2\Omega\text{cm}^2$, $C_d = 50\,\mu\text{F cm}^{-2}$, $k_{-1} = 48$, $k_2 = 5.6 \times 10^4$, $k_{-2} = 10^6$, and for different rotation rates. The characteristic frequencies of the first two loops are indicated.

On the other hand, a model based only on a partial blocking of the interface would provide a diagram of similar shape as those displayed in Fig. 8, but the intermediate loop should be reducible vs p exactly as the one in the low frequency range; therefore, the intermediate dependence, between those two limit situations, observed on p, can reflect the occurrence of both causes as this will be confirmed by the EHD impedance.

For both potentials, -150 and -200 mV, the agreement between R_p and the slope of current–potential curves is very good at all rotation rates.

4.2.2. EHD impedance. A continuous trend of the diagrams is clearly visible with the current. The reducibility vs p which is bad for different Ω values at low anodic current (Fig. 9A, $I = 5\,\mu$A) becomes better when I is increased (Fig. 9B and 9C) and is quite satisfactory for the larger current investigated ($I = 150\,\mu$A, Fig. 9D). In the low frequency range, these impedance diagrams are characteristic of a mass transport through a porous layer. The effect of this layer (Cu_2O grown at E_{corr} before polarizing the electrode at anodic potential) is important close to E_{corr} and decreases for current more and more anodic. At the highest current all the layer effect disappears and the interface can be considered as free of Cu_2O in good agreement with the previous a.c. impedance measurements.

At all currents the impedance values at the lowest rotation rate agree very well with the theoretical expression and give the best fit for a Schmidt number close to 2000. Considering the properties of EHD impedance in galvanostatic mode, the Sc fitted value is likely to be that of the involved diffusing species, $CuCl_2^-$ in the present case, when the rotation rate is very low. Taking an average value $Sc = 2000$ and for $\nu = 8.93 \times 10^{-3}\text{cm}^2\text{s}^{-1}$, one finds $D = 4.5 \times 10^{-6}\text{ cm}^2\text{ s}^{-1}$. This value is of the order of that found by Smyrl [5] and equal to $5.68 \times 10^{-6}\text{ cm}^2\text{ s}^{-1}$. If we compare these results to our model (Equation 9) we find a good agreement because the effect of the [CuCl] relaxation corresponding to the factor $1/(j\omega + k_2[Cl^-])$ appears at higher frequency according to the a.c. impedance measurement.

In the high frequency range, at all mean currents, the experimental diagrams deviate from the theoretical expression and display in particular a decrease of the phase shift as p is higher. This effect is similar to a partially blocked surface effect where only the transition region is visible, a region where the diagrams are not reducible by the dimensionless frequency p. In this case we may assume that the interface is partially covered by Cu_2O and the part which is not covered plays for the EHD impedance a role which is similar to an active site on a partially blocked electrode.

4.3. *Corrosion potential*

4.3.1. A.c. impedance. At the corrosion potential a.c. impedance experiments were run only after a long rest

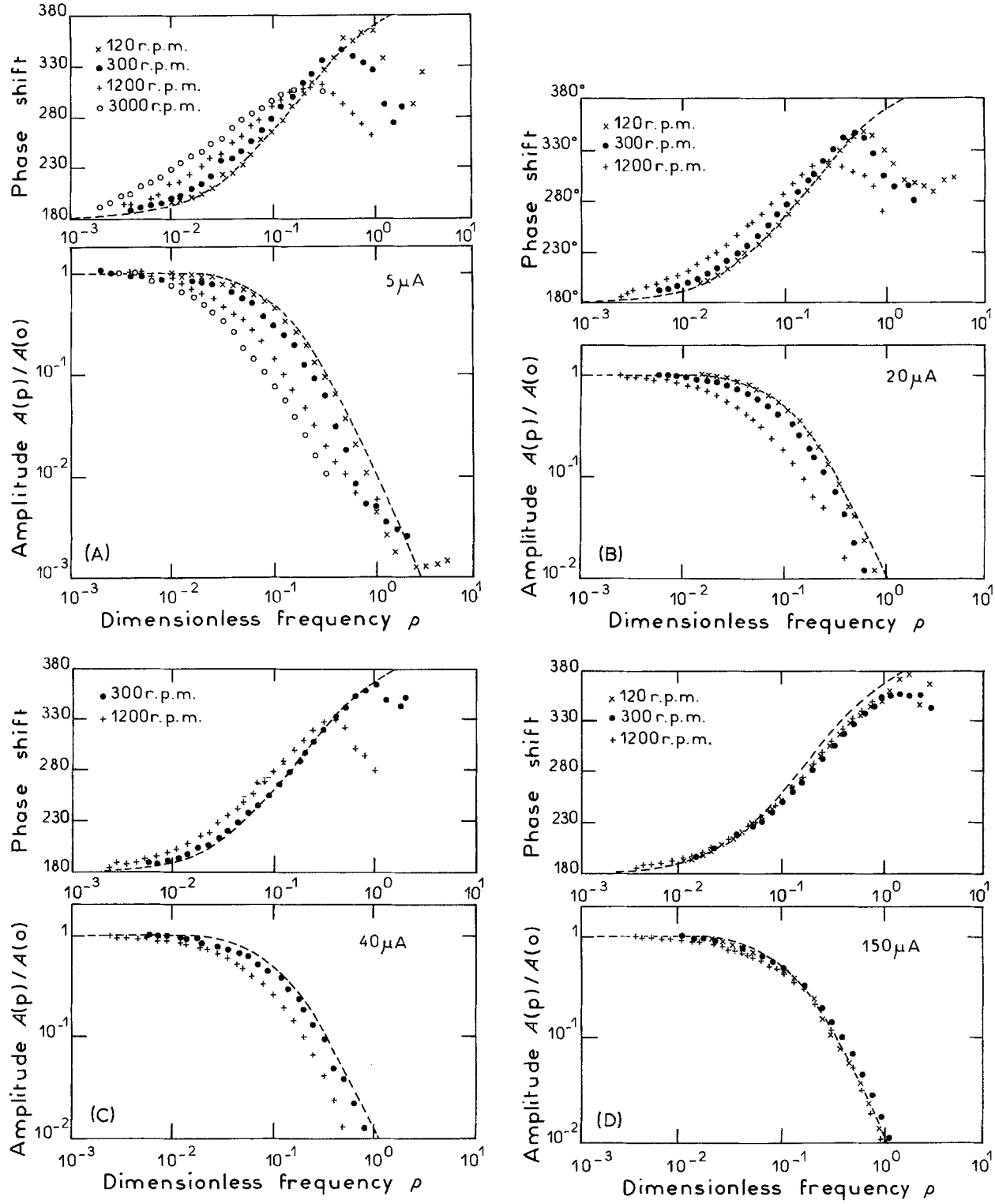

Fig. 9. EHD impedance in galvanostatic regulation for different anodic currents. The theoretical curve corresponding to $Sc = 2000$ is reported as a dashed line.

time; the electrode was kept at open circuit for 16 h or more under stationary conditions and then rotated at the appropriate $\bar{\Omega}$ for a time long enough to achieve a stable value of E_{corr} (2–4 h). A.c. impedance diagrams after short immersion times, i.e. when the evolution of E_{corr} is fast compared with the duration of the experiment (1 h), were not recorded.

Impedance plots obtained after 16 h at 300, 1000 and 3000 rpm are shown in Fig. 10. Two poorly separated loops are visible at each Ω. The R_p values obtained by a.c. impedance (also for other Ω values than those of Fig. 10) are in fair agreement with those of Fig. 9 in Part I, procedure A.

In all the diagrams of Fig. 10 the low frequency loop is ascribed to mass transfer. However, in this instance, the characteristic frequencies are somewhat lower than those of Fig. 7 (anodic range). Even lower values are found for the characteristic frequencies of the low frequency loops of the a.c. impedance plots obtained after 100 h at E_{corr}. In addition, after such a time, a plot of Z_{im} vs p on bilogarithmic scales (Fig. 11) indicates that the characteristic reduced frequency is

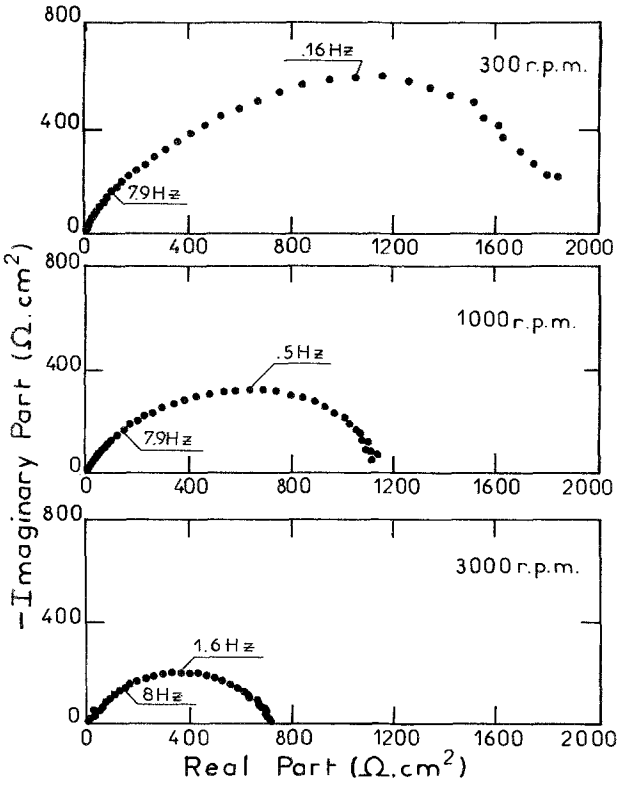

Fig. 10. A.c. impedance diagrams at the corrosion potential obtained after 16 h for different rotation rates. The characteristic frequencies are indicated.

lower the higher $\bar{\Omega}$. Such a shift is most likely a consequence of diffusion through a porous layer.

After recording each diagram of Fig. 10 the electrolyte was purged with nitrogen, while keeping the electrode potential constant. This way, after removal of oxygen, a net anodic current was flowing. A.c. impedance diagrams were recorded again under these conditions. Both the shapes of the diagrams and the characteristic frequencies are only slightly changed with respect to aerated solutions (see, for instance, for $\bar{\Omega}$ = 1000 rpm, Fig. 12). In Part I we assumed that $R_{t_c} = 3R_{p_a}$ and so at $\omega = 0$, $Zf(o) = (3/4)R_{p_a}(o)$. By removing oxygen and keeping the potential constant the faradaic impedance at zero frequency becomes $R_{p_a}(o)$, i.e. ~30% higher.

Experimentally we find an increase of ~20% which means that R_{t_c} is 5 times larger than R_{p_a}. The anodic impedance decreases when ω increases while the cathodic one is constant, so in the high frequency range R_{t_c} is much larger than $Z_a(\omega)$ and may be neglected, in agreement with experimental data.

Thus, it may be concluded that the a.c. impedance plots obtained at E_{corr} are due mainly to the anodic partial reaction involving mass transfer occurring through a porous layer of Cu_2O. Simulated curves obtained for the same Ω values, the same parameters used for the simulation at $E = -150$ mV and a constant E_{corr} (assumed for this simulation as independent of Ω and $= -250$ mV), are presented in Fig. 13. Only two loops are clearly visible. The one at high frequency is due to modulation of [CuCl] since that due to R_t is negligible. By comparing the simulated curves at -150 mV and E_{corr} a shift of the characteristic frequency of the low frequency loop is observed due to a coupling of the loops due to [CuCl] modulation and to mass transfer. Such a shift is lower than that found experimentally which must be due in part to diffusion through a porous layer. As in the anodic range, the experimental plots are flattened with respect to the simulated ones, most likely because of dispersion phenomena.

4.3.2. EHD impedance. For the same reasons of fast interface evolution given for the a.c. impedance, EHD impedance diagrams after short immersion time were not recorded.

EHD impedance measurements obtained with galvanostatic regulation ($I = 0$) after long exposure times, 64 h, are presented in Fig. 14. The impedances recorded at different rotation rates are not reducible by the usual dimensionless frequency p and the phase shift increases continuously with p. The two properties are characteristic of a layer effect as previously mentioned [15]. The phase shift variation also indicates a clear anodic response and, when the rotation rate is small, the corresponding curve approaches the theoretical curve calculated for $Sc = 2000$. We may conclude that $CuCl_2^-$ diffuses in the electrolyte and

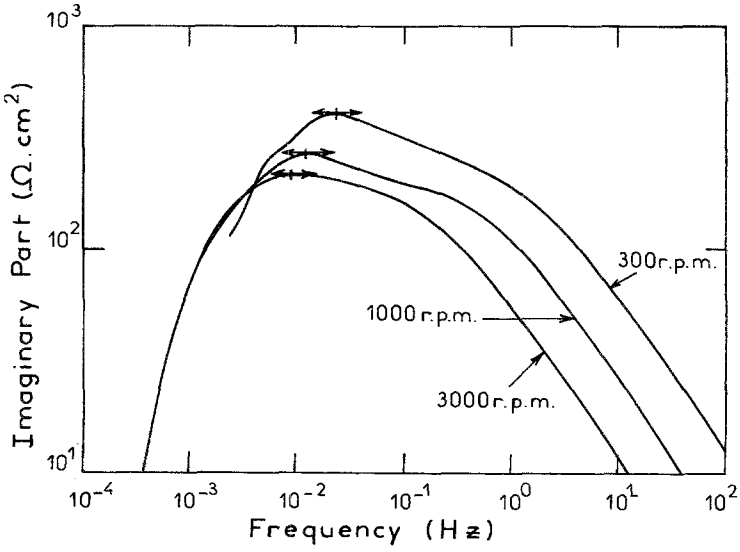

Fig. 11. Variation of the imaginary part of the a.c. impedance vs the dimensionless frequency p. Data obtained after 100 h at E_{corr}.

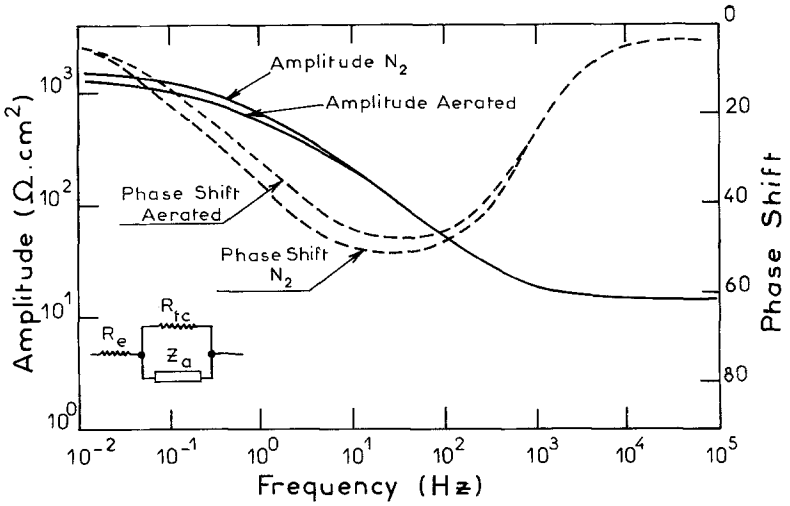

Fig. 12. Comparison, in Bode coordinates, of the a.c. impedance obtained at the same potential in aerated solution and after purging with N_2. The electric scheme of the interface is given; R_{tc} corresponds to Equation 18 and Z_a to Equation 17 of Part I.

through the Cu_2O layer in good agreement with the analysis of the a.c. impedance.

5. Conclusion

Most of the experimental results were discussed in the previous section and in the discussion of Part I. Therefore, only a brief summary of the main conclusions reached with the present investigation is necessary.

The cathodic partial reaction is described, in good agreement with all steady-state and impedance measurements, as due to oxygen reduction:

$$O_2 + 2H_2O + 4e^- \rightleftharpoons 4OH^-$$

On the cathodic plateau we have shown that there is no effect due to the Cu_2O layer and the interface may be considered as uniformly accessible for oxygen reduction. The diffusion coefficient measured by EHD impedance technique is $1.4 \times 10^{-5}\,cm^2\,s^{-1}$ in good agreement with the literature [19].

We found that the behaviour of the system in the potential range between the CuCl reduction and E_{corr} is not fully reproducible (see Part I). EHD response seems to be due to a layer effect (CuCl) combined with that of a partially blocked interface. It is clear that the diffusing species is oxygen.

In the anodic range, a model involving the following elementary steps:

$$Cu + Cl^- \rightleftharpoons CuCl + e^- \underset{-Cl^-}{\overset{+Cl^-}{\rightleftharpoons}} CuCl_2^-$$

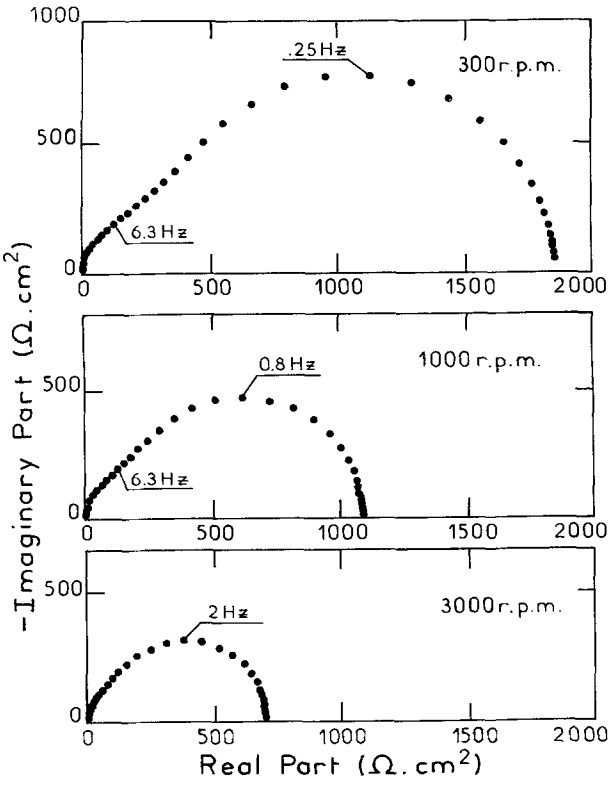

Fig. 13. Simulated a.c. impedance diagrams from Equation 9 for $R_t = 14\,\Omega cm^2$, the same kinetic constants of Fig. 8 and $E = -250\,mV$.

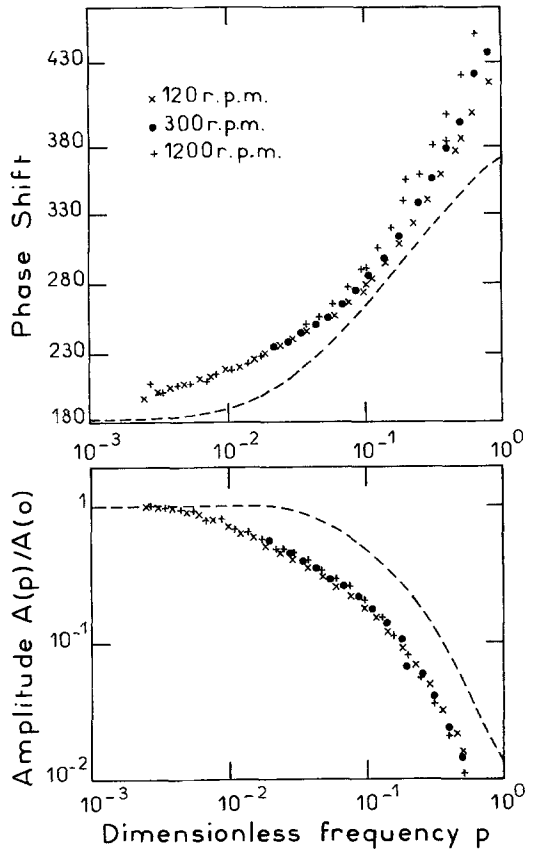

Fig. 14. EHD impedance in galvanostatic regulation obtained after 64 h at E_{corr}. The phase shift indicates an anodic behaviour.

was found to be able to explain both steady-state results and impedance experiments carried out at large anodic currents. Anodic mass transfer seems to occur in conditions of uniform accessibility and thus it is possible to determine the value of the diffusion coefficient of $CuCl_2^-$ (4.5×10^{-6} cm^2 s^{-1}). The parallel path leading to the formation of Cu_2O by hydrolysis of CuCl was not taken into account in our quantitative kinetic analysis because it is a much slower process than all other steps; only an effect of Cu_2O as an insoluble product was claimed for small anodic currents. We think that such an effect becomes increasingly less important at higher currents due to a fast renewal of the electrode surface. At the corrosion potentials, the hydrolysis reaction can also be neglected from the kinetic point of view. However, the effect of the Cu_2O layer on the mass transfer must be considered for explaining the experimental results obtained after long exposure time. Under these conditions the Cu_2O layer may be assumed to undergo no change of thickness during the time of an experiment. Its growth (on a long time scale) explains the increase of R_p with time and the progressive shift towards lower values of the characteristic frequency of the mass transfer response in a.c. impedance experiments. All our data suggest that the anodic current is mass transfer-limited by the diffusion of $CuCl_2^-$ through both the Cu_2O layer and the electrolyte, while the cathodic current is purely a kinetic current.

Except for the effect of the surface layer the model for the anodic electrodissolution presented in Part I and developed in Part II for the impedance measurements may also explain qualitatively the behaviour at the corrosion potential.

References

[1] C. Deslouis, G. Mengoli, M. M. Musiani and B. Tribollet, *J. Appl. Electrochem.* **18** (1988) 374.
[2] A. L. Bacarella and J. C. Griess, *J. Electrochem. Soc.* **120** (1973) 459.
[3] A. Moreau, J. P. Frayret, F. Del Rey and R. Pointeau, *Electrochim. Acta* **27** (1982) 1281.
[4] B. Tribollet and J. Newman, *J. Electrochem. Soc.* **131** (1984) 2780.
[5] W. H. Smyrl, *J. Electrochem. Soc.* **132** (1985) 1556, 1563.
[6] H. P. Lee and K. Nobe, *J. Electrochem. Soc.* **133** (1986) 2035.
[7] El-Taib Heakal and S. Haruyama, *Corros. Sci.* **20** (1980) 887.
[8] F. Mansfeld, M. W. Kendig and S. Tsai, *Corrosion* **38** (1982) 570.
[9] K. Tokuda, S. Bruckenstein and B. Miller, *J. Electrochem. Soc.* **122** (1975) 1316.
[10] C. Deslouis, C. Gabrielli, Ph. Sainte-Rose Fanchine and B. Tribollet, *J. Electrochem. Soc.* **129** (1982) 107.
[11] B. Tribollet and J. Newman, *J. Electrochem. Soc.* **130** (1983) 2016.
[12] C. Deslouis and B. Tribollet, *Mat. Sci. Forum* **8** (1986) 1.
[13] C. Deslouis, C. Gabrielli and B. Tribollet, Electrochem. Soc. Meeting, New Orleans, Louisiana (1984) Ext. Abs. 261.
[14] C. Deslouis, I. Epelboin, C. Gabrielli, Ph. Sainte-Rose Fanchine and B. Tribollet, *J. Electroanal. Chem.* **107** (1980) 193.
[15] C. Deslouis, B. Tribollet, M. Duprat and F. Moran, *J. Electrochem. Soc.*, **134** (1987) 2496.
[16] C. Deslouis and B. Tribollet, *J. Electroanal. Chem.* **238** (1987) 67.
[17] B. Tribollet and J. Newman, *J. Electroanal. Soc.* **130** (1983) 822.
[18] C. Deslouis, C. Gabrielli and B. Tribollet, *J. Electrochem. Soc.* **130** (1983) 2044.
[19] F. Opekar and P. Beran, *J. Electroanal. Chem.* **69** (1976) 1.